We are IntechOpen,
the world's leading publisher of
Open Access books
Built by scientists, for scientists

6,400
Open access books available

174,000
International authors and editors

190M
Downloads

Our authors are among the

154
Countries delivered to

TOP 1%
most cited scientists

12.2%
Contributors from top 500 universities

CLARIVATE ANALYTICS
BOOK CITATION INDEX
INDEXED

WEB OF SCIENCE™

Selection of our books indexed in the Book Citation Index
in Web of Science™ Core Collection (BKCI)

Interested in publishing with us?
Contact book.department@intechopen.com

Numbers displayed above are based on latest data collected.
For more information visit www.intechopen.com

Chapter

Graphene-Based Plasmonic Terahertz Laser Transistors

Taiichi Otsuji

Abstract

This chapter reviews recent advances in the research of graphene-based plasmonic terahertz laser transistors. Optically or electrically pumped graphene works as a gain medium in the terahertz frequency range. The author's group theoretically discovered this fact and experimentally verified the single mode terahertz emission, as well as broadband terahertz amplified spontaneous emission from fabricated graphene-channel field-effect transistor (GFET) laser chips. However, its lasing threshold temperature was low (100 K) and emission intensity was weak. To drastically improve the laser performance, the introduction of graphene Dirac plasmons (GDPs) as the gain booster is promising. The author's group found a novel way to promote the current-driven instability of the GDPs in an asymmetric dual-grating-gate GFET, demonstrating room-temperature amplification of stimulated emission of terahertz radiation with the maximal gain of 9% which is four times larger than the quantum-mechanical limit when terahertz photons directly interact with graphene electrons without excitation of the GDPs. The author also proposes the active controlling of the parity and time-reversal symmetries of the GDPs as a paradigm towards ultrafast direct gain switching in the GFET lasers. Future directions to unite the gain seed and amplifier sections in a single GFET structure will be addressed with several feasible scenarios.

Keywords: graphene, plasmon, terahertz, laser, transistor, instability, PT-symmetry

1. Introduction

Exploitation of the electromagnetic resources in the terahertz (THz) spectra is the fundamental need to envision a real-world future smart society based on innovative information and communication technology (ICT) which will be led by the next generation 6G and 7G wireless communication systems [1]. However, the THz region is still under exploration due to substantial physical limitations for both electron devices such as transistors, and photonic devices such as lasers [1, 2]. Low-power consumed, integrated, room-temperature operating novel solid-state THz laser devices is the critical demand for the brighter future society [3]. In such a situation, graphene, a monoatomic layer of sp^2-bonded carbons in a honeycomb crystal lattice, has drawn considerable attention due to its unique and superior

carrier transport, optical, and plasmonic properties since it has been discovered [4–9].

Electrons and holes in graphene hold a linear dispersion relation with zero bandgap, resulting in extraordinary features like massless relativistic Dirac fermions with back-scattering-free ultrafast transport [4–6] as well as the negative-dynamic conductivity in the THz spectral range under optical or electrical pumping [9–11]. The author's group succeeded in single-mode emission at 5.2 THz and 1–8-THz broadband amplified spontaneous emission at 100 K from fabricated graphene-channel laser transistors [12]. However, its gain and output intensity are thoroughly limited by the absorption coefficient of monolayer graphene below 2.3% [9, 11]. To break through the substantial limit, graphene Dirac plasmons (GDPs) open a pathway toward the realization of intense THz laser transistors operating at room temperatures with dry-cell battery [7, 13, 14]. The physics behind the GDPs is the current-driven instabilities giving rise to self-oscillation and coherent amplification in the THz electromagnetic spectra [15–18]. In this chapter, the theory and experiments for graphene-based plasmonic terahertz laser transistors are reviewed.

2. Graphene THz laser transistors under current-injection pumping

2.1 Theory and modeling

When the intrinsic graphene is optically pumped with a photon energy $\hbar\Omega$, where $\hbar$ is the reduced Planck constant and Ω is the angular frequency of photon, interband transitions lead to the generation of "hot" photoelectron-photohole pairs in the distance equal to the photon energy at above and below the Dirac point for the electrons and holes, respectively (**Figure 1**). At room temperature, these photo-excited "hot" electrons and "hot" holes are quasi-equilibrated with the low-energy conduction electrons and valence holes around the Dirac point at the ultrafast time scale of tens of femtoseconds due to the carrier-carrier scattering resulting in the quasi-Fermi distribution (**Figure 1**) [11, 19]. As a result, the quasi-Fermi level of electrons and holes split and shift *below* and *above* the Dirac point, respectively. At the same time, the high-energy electrons and holes, lose their energy by emitting optical phonons. Thus the quasi-Fermi distribution, which is originally widely spread in the energy space, gets concentrated around the Dirac point. This results in a rapid recovery of the quasi-Fermi level on a picosecond time scale [19]. After the energy relaxation via the optical phonon emissions, the non-equilibrium electrons and holes may lose their energies via the "interband" optical phonon scattering, impurity−/disordered scattering, as well as the acoustic phonon scattering, or they recombine. Compared to the aforementioned "intraband" optical phonon scattering, these scattering and recombination processes have much longer relaxation times. Therefore, the nonequilibrium carriers are piled up around the Dirac point if the pumping intensity is sufficiently high. This is the carrier population inversion, in which the quasi-Fermi levels for electrons and holes shift *above* and *below* the Dirac point, respectively (**Figure 1**). The Auger-type three-particle scattering processes are theoretically forbidden in the ideal graphene [20], but they might dominate in the disordered low-quality graphene and/or under intense pumping leading to significant many-body effects [21]. Thus, the Auger-type scattering is recognized as a killer of the carrier population inversion [22]. However, the carrier population
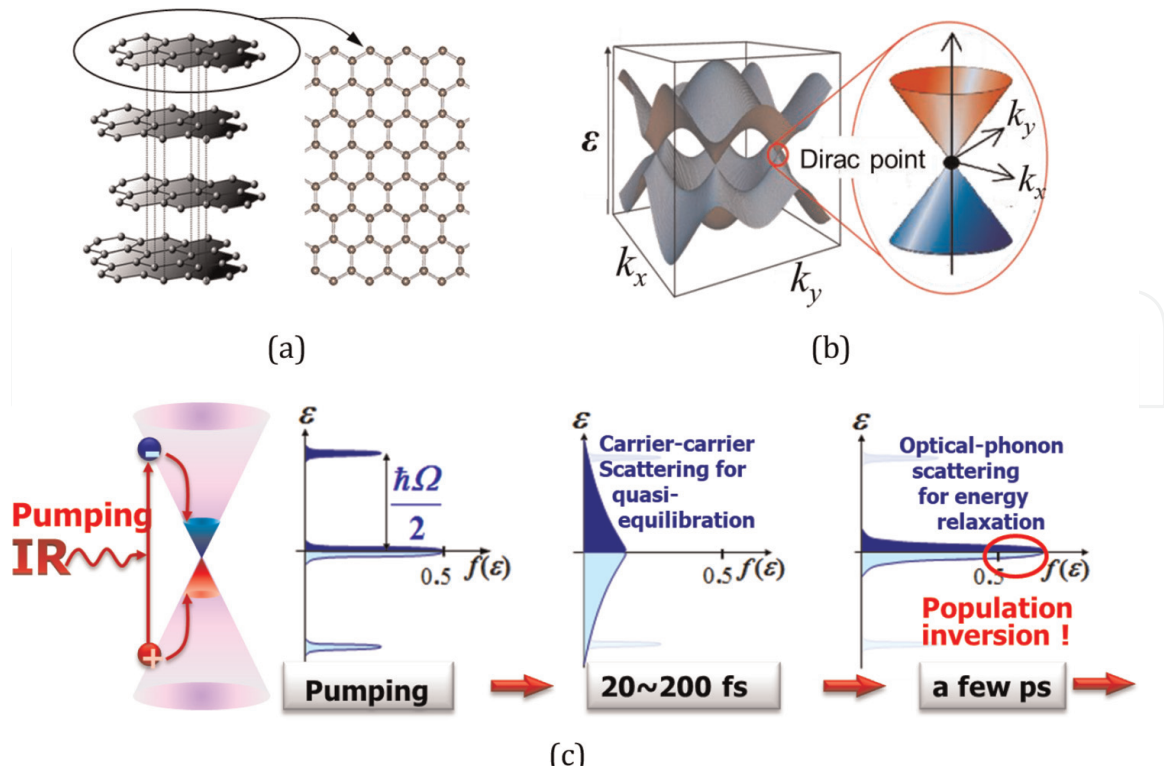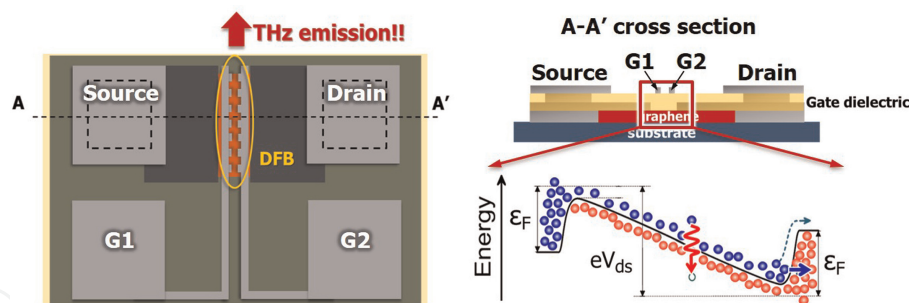
Figure 1.
Graphene and its carrier energy relaxation dynamics under optical pumpinp. (a) Real-space lattice image from bulk graphite (left) to graphene (right). (b) Energy band structure of graphene. (c) Carrier energy relaxation dynamics of intrinsic graphene under optical pumping. When graphene is optically pumped with a photon energy ħΩ photoelectron-photohole pairs are generated at the level ħΩ/2 above and below the Dirac point, and then followed by ultrafast carrier-carrier scattering and then optical phonon scattering. Adapted with permission by IEEE from Ref. [11].

inversion in the THz frequency range has been experimentally observed in prolonged long time more than 1 ps after a rather intense pumping with a high photon-energy (∼1.5 eV) picosecond laser pulses in high-quality epitaxial graphene even at room temperature [23]. This result encouraged us to explore the creation of the graphene THz lasers/amplifiers.

Optical pumping suffers from significant heating of the electron-hole plasma suppressing carrier population inversion. The electron-hole plasma, however, can be cooled down if the pumping photon energies are sufficiently low. Recently rigorous theoretical modeling and calculation of the Auger scattering rate including many-body effects of Coulomb interactions reveal that the Auger scattering is substantially suppressed when carrier temperature is maintained at or below room temperature [24]. In this situation, current injection pumping is the idealistic way to suppress the carrier heating decreasing the pumping threshold because the pumping energy could be of the order of millielectron volts in a graphene p-i-n junction structure [10, 11].

A dual gate p-i-n structure using a graphene-channel field effect transistor (DG-GFET) has been proposed as the simplest current-injection THz graphene laser structure (**Figure 2**) [10, 12]. The conductivity profiles calculated for the typical dimensions and applied bias conditions demonstrate the advantage of current-injection pumping compared to optical pumping. The optical conductivity of the graphene channel under the gates and drain biases is given by [10, 12]:

Figure 2.
DG-GFET (dual-gate graphene-channel field effect transistor). Top view (left), cross-sectional view (right upper), and a band diagram under complementary dual gate bias and forward drain-source bias condition getting population inversion and resultant spontaneous THz emission (right lower). A distributed feed-back (DFB) laser cavity is incorporated in the toothbrush-shaped dual gate electrodes in which the distance between the gates is periodically modulated to modulate the gain coefficient, producing resonant modes to the THz photons propagating along the DFB cavity (in plane DG finger direction). The DFB period gives the resonant mode frequencies and the modulation depth and the number of periods give the quality factor of the cavity [12].

$$\sigma_\omega = \sigma_\omega^{\text{intra}} + \sigma_\omega^{\text{inter}}, \tag{1}$$

$$\sigma_\omega^{\text{intra}} \approx \frac{e^2 \varepsilon_F}{2\pi\hbar^2} \cdot \frac{\tau}{1 + \omega^2\tau^2}, \tag{2}$$

$$\sigma_\omega^{\text{inter}} \approx \frac{e^2}{2\hbar} \cdot exp\left(\frac{eV - 2e\sqrt{V_F V_g}}{2k_B T}\right) \cdot \sinh\left(\frac{\hbar\omega - eV_{ds}}{2k_B T}\right), \tag{3}$$

where $\sigma_\omega^{\text{intra}}$ and $\sigma_\omega^{\text{inter}}$ are the intraband and interband components of the conductivity, respectively, e is the elementary charge, ε_F is the Fermi energy reflecting the carrier doping level by applying V_g, τ is the carrier momentum relaxation time, k_B is the Boltzmann constant, and T is the temperature [10]. The gate biasing ($\pm V_g$) controls the injection level, whereas the drain bias (V_{ds}) controls the level of population inversion (the amount of shifting the quasi-Fermi levels of electrons and holes). To minimize the undesired tunneling current lowering the injection efficiency the distance between the dual gate electrodes should be sufficiently long. When the carrier momentum relaxation time is rather long ($\tau = 2.0$ ps) and carrier injection level is pertinent at $V_g = 1.0$ V, an even weak V_{ds} produces a net gain (negative conductivity) in a wide THz frequency range (**Figure 3a**) [12]. The situation dramatically changes when the value of τ becomes short (down to 0.1 ps); in this case, the net gain almost disappears (**Figure 3b**) [12]. As a consequence, the high-quality graphene having a picosecond-order value of τ is mandatory to obtain a net gain in the THz range. It is noted that the maximal available negative conductivity is limited below $e^2/(4\hbar)$ corresponding to the interband absorption coefficient ($\alpha = \pi e^2/(c\hbar) \approx 2.3\%$) of monolayer graphene [9].

2.2 Experiments

The author's group designed and fabricated the DG-GFETs incorporating a distributed feed-back (DFB) type internal cavity, demonstrating the world-first observation of single-mode lasing from GFETs at 5.2 THz at 100 K (**Figure 4**) [12]. The graphene used in the GFETs is non-Bernal-stacked a few layers of high-quality graphene synthesized by the thermal decomposition of a C-face 4H-SiC substrate. The GFET was fabricated using a standard photolithography and a gate stack with a SiN
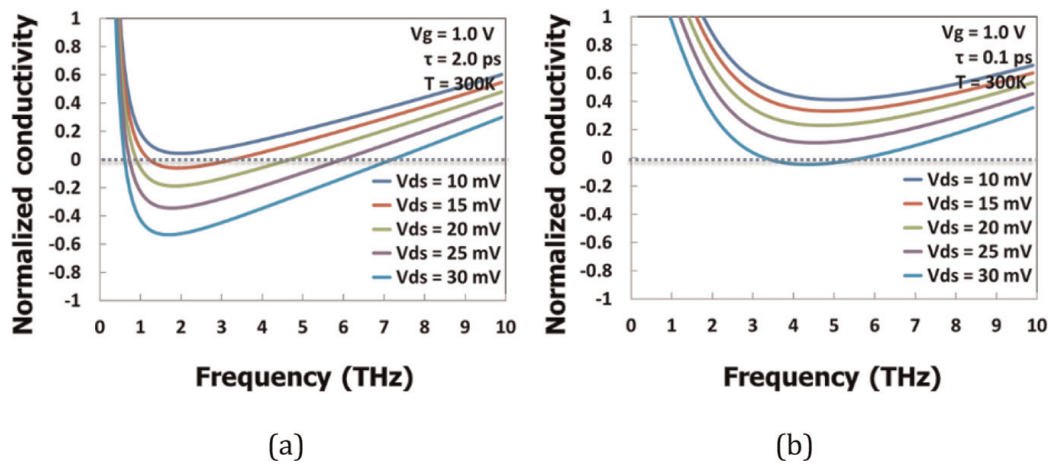
Figure 3.
Real part of the conductivity spectra of a complementary dual-gate bias DG-GFET at 300 K with varying drain-source bias voltage. The vertical axis is normalized by the fundamental conductivity ($e2/4h$), which corresponds to 2.3% absorbance of monolayer graphene. Vg (= − Vg1 = +Vg2) = 1.0 V. (a) τ = 2.0 ps. (b) τ = 0.1 ps. Adapted with permission by the authors under the creative commons attribution CC-BY 4.0 international license from Ref. [12].

dielectric layer providing an excellent intrinsic field-effect mobility exceeding 100,000 cm^2/Vs at 300 K. A pair of toothbrush-shaped gate electrodes was patterned to form a DFB cavity in which the active gain area and corresponding gain coefficient were spatially and periodically modulated. The THz single mode lasing was observed at around 5.2 THz with an emission intensity as high as 0.1 μW and with a linewidth of 31 GHz under pertinent complementary DG biases ($\pm V_g$) and V_{ds} conditions serving the carrier population inversion in good agreement with numerical simulations (**Figure 4a**). A different sample with the identical design on the same wafer exhibited an amplified spontaneous broadband emission ranging from 1 to 7.6 THz at 100 K with a maximal emission power of 80 μW (**Figure 4b**).

2.3 Discussion toward introduction of graphene plasmons

Figure 4 shows the variation of THz emission characteristics stems from a poor THz photon field confinement and resultant weak gain overlapping. Numerical analysis well reproduces such a variation when a wide fraction of the carrier momentum relaxation time of graphene carrier under weak gain overlapping conditions is assumed [12, 25]. Improvement in the gain overlapping by introducing a plasmonic waveguide for dense THz photon field confinement as well as on the cavity quality factor by increasing the number of the DFB periods and the DFB modulation depth will lead to more intense lasing at higher temperatures approaching 300 K [25]. Also, the introduction of the GDP dynamics is a promising way to dramatically increase the THz net gain and quantum efficiency of the GFET lasers. Due to the extremely slow-wave nature (by two orders slower than the speed of light) of the GDPs [7, 8]. Once THz photons couple with the graphene plasmons, photons may propagate along the population-inverted graphene as plasmon polaritons having the plasmon velocity so that the interaction between the THz photons and graphene carriers is dramatically enhanced in proportion to the ratio of the speed of photon to that of the plasmon, well exceeding the aforementioned quantum-mechanical limit of 2.3% per layer of graphene [26]. A giant gain enhancement of up
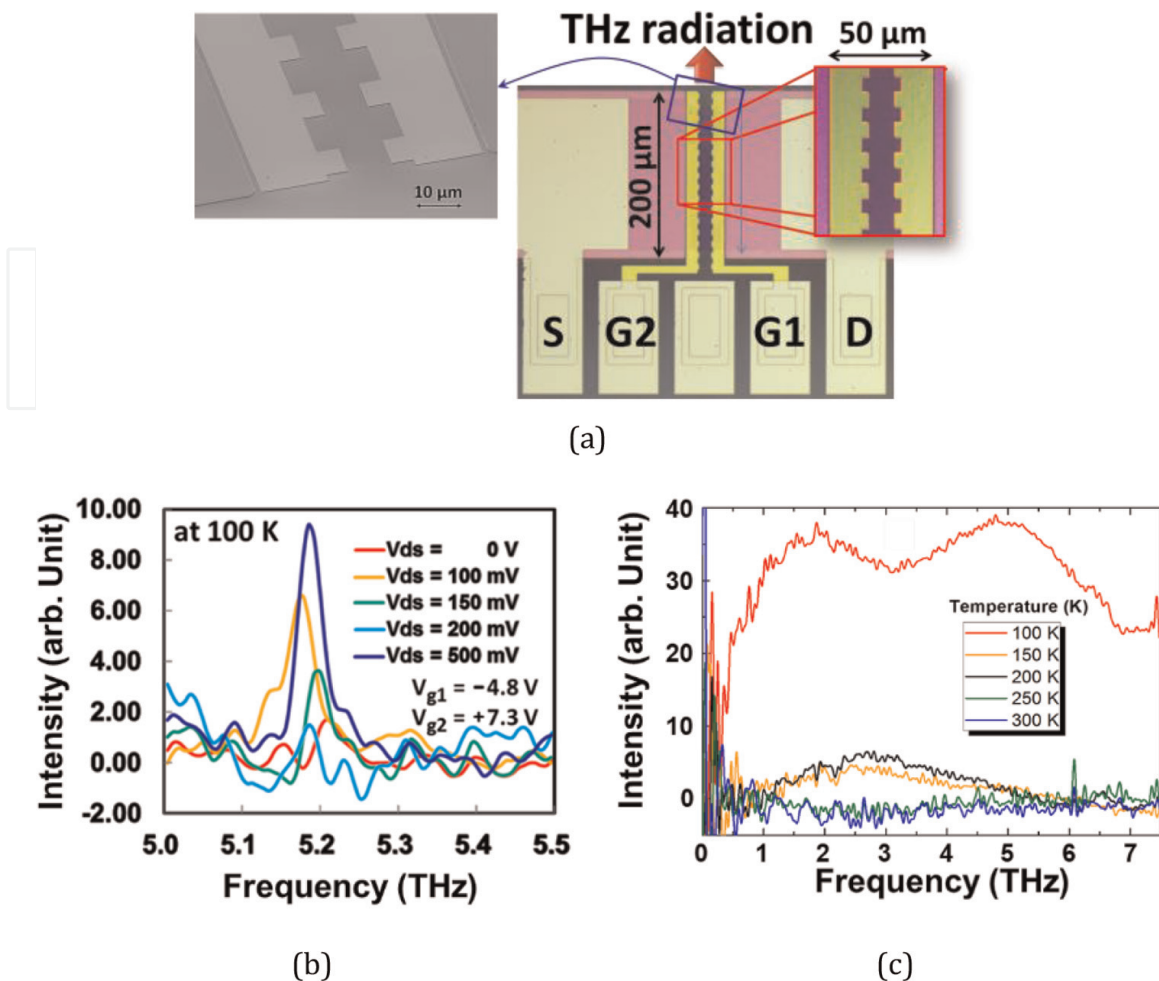
(a)

(b)

(c)

Figure 4.
Measured emission spectra from fabricated DFB-DG-GFET samples. (a) Electron scanning and optical microphotographic images of a fabricated sample. (b) Single-mode emission at ~5.2 THz at 100 K with a ~ 0.1 μW and a minimal linewidth of ~31 GHz from one fabricated DFB-DG-GFET sample. (c) Amplified broadband spontaneous emission in a frequency range from 1 to 7.6 THz at 100 K from a different DFB-DG-GFET sample. The threshold operating temperature stays in between 100 and 150 K. Adapted with permission by the authors under the Creative Commons Attribution CC-BY 4.0 International license from Ref. [12].

to 50 times as high as that without graphene plasmons has been experimentally observed in the THz range [27].

3. Graphene-plasmonic instabilities for THz amplification

3.1 Theory and modeling

Unlike plasmons in the bulk, two-dimensional plasmons have a wavenumber dependence, and when they are localized only by an in-plane crystal field on a two-dimensional surface (non-gate-controlled plasmons) or electrostatically by an external vertical electric field (gate-controlled plasmons), as in a transistor gate structure, their dispersion relations are different [7, 28]. Furthermore, the plasmon dispersion relation is different between ordinary two-dimensional electron systems, which have a quadratic dispersion relation due to the existence of electron effective mass, and Dirac two-dimensional electron systems, which have linear dispersion due to the

disappearance of electron effective mass, such as electrons in graphene [28]. However, for the electron concentration, the plasmon energy is proportional to the 1/4 power of the electron concentration due to the peculiarity of the linear dispersion of the Dirac electrons [7, 28]. When plasmon is localized in the element structure, the plasmon mode stands at a specific frequency determined by the structural dimensions and the plasmon velocity, and if the structural dimensions are less than or equal to the average free pass of the electrons, the plasmon coherency is conserved and plasmon resonance is promoted.

When plasmon is excited in a two-dimensional electron system traveling in direct current within a limited region such as the channel in a transistor, the difference between the electron drift velocity and the plasmon velocity modulates the spatio-temporal density of the plasmon. At the boundary edges of this region, although the electron travel is guaranteed its continuity by the current continuity condition, the plasmon (plasma wave) is subject to reflection due to impedance mismatch at the boundaries. As a result, a standing wave is generated by the superposition of the forward-traveling waves and the reflected backward waves. When the singular or multiple wavelength(s) of the plasma waves meet the channel length, the amplitude of the plasmon increases divergently with each repeated reflection, and the plasmon falls into an unstable state. This phenomenon is called plasmon instability and is a self-excited oscillation phenomenon that occurs when the DC energy of the electron is converted to plasmon energy near the resonance frequencies [15, 28].

Plasmon instability has multiple mechanisms for its occurrence, depending on the relationship between the electron drift velocity v_d and the plasmon velocity s. Under the condition $v_d < s$, which is generally established, there are two types of instability; Dyakonov-Shur (D-S) instability [15] and Ryzhii-Satou-Shur (R-S-S) instability [16]. In case of the D-S instability, the plasma wave amplitude increases with each reflection at the open end where the reflection coefficient is close to 1 due to the Doppler shift effect associated with the asymmetry of the plasmon boundary, whereas the R-S-S instability is caused by electron bunching effects due to electrons traveling at different drift velocities inside the plasmon resonator at high electron concentration and outside the resonator at low electron concentration. At the boundary where the drift velocity exceeds the plasmon velocity, $v_d > s$, a plasmon shock wave type instability (plasmonic boom instability) [17] as well as the R-S-S type, and furthermore, within a periodic electron concentration modulation structure, a Cherenkov-type instability, where the plasmon bunching is divergently enhanced, are observed, respectively [17].

We have proposed a graphene-channel field-effect transistor with an "asymmetric dual-grating-gate" (ADGG-GFET), in which a broadband antenna mechanism that efficiently couples terahertz electromagnetic waves and graphene plasmon are woven into the transistor electrodes [29]. The ADGG consists of two independent gate electrodes, G1 and G2, arranged in an interdigitated manner (**Figure 5a**). A high bias is applied to one G1 to accumulate highly concentrated electrons in the channel region below G1, and a Dirac potential is applied to the other G2 to deplete the channel region below G2, periodically modulating the electron concentration in the channel (**Figure 5b**). In this situation, when a DC bias is applied to the drain, the electron drift velocity is also periodically modulated in response to the spatial distribution of the electron concentration in the channel to preserve the current-continuity condition. As a result, the plasmon instability described above is excited. The high electron concentration region functions as a plasmon resonator, leading to the self-excited oscillation of plasmon near the plasmon resonance frequency. The plasmon itself is a
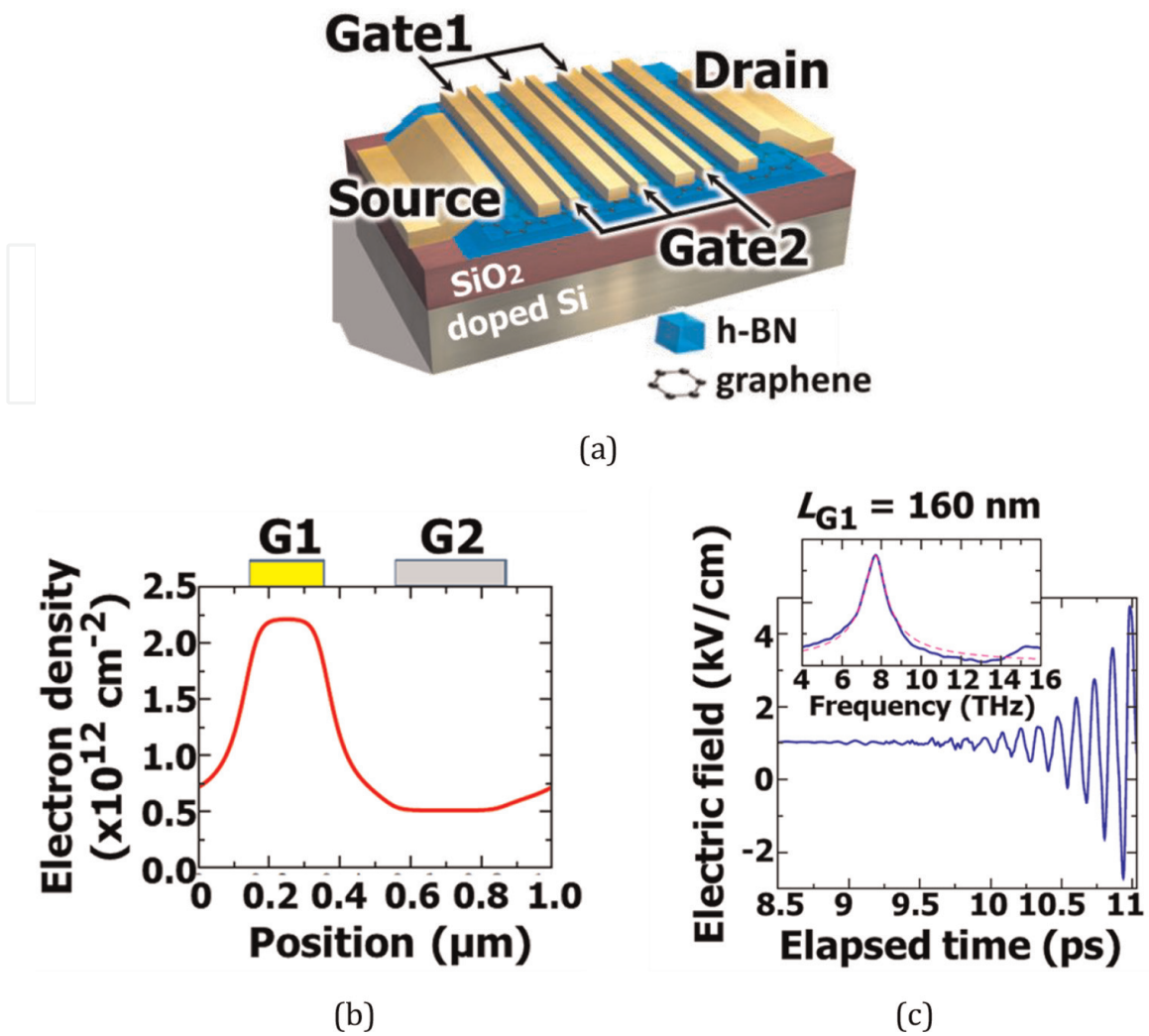
(a)

(b)   (c)

Figure 5.
An example of numerical analysis of plasmon instability in an ADGG-GFET. (a) A bird's eye schematic of an outlook of the ADGG-GFET. (b) Spatial density modulation of electrons in a unit section of the ADGG structure. The high-electron-density region underneath G1 works as a plasmonic cavity whereas the low-electron-density region underneath G2 serves a high-speed electron transit region and works to excite plasmons in the cavity. Adapted with permission by American Physical Society from Ref. [30]. (c) Numerically simulated temporal evolution of the longitudinal electric field intensity after turning on the DC drain bias beyond the threshold level, leading to coherent self-oscillation at the frequency of plasmon resonance determined by the cavity length L_{G1} and the electron densities in the cavity. Adapted with permission by American Physical Society from Ref. [30].

non-radiative evanescent wave, but it is converted into an electromagnetic wave through the antenna mechanism of ADGG, leading to free-space radiation. If the plasmon cavity length (width of each finger) of the gate grating electrodes is set to submicron dimensions, self-excited oscillation in the THz band can be obtained. If a THz wave with a frequency component near the oscillation frequency is injected from the outside, the injection locking synchronization phenomenon will be activated and the self-excited oscillation will coherently synchronize with the injected terahertz wave. As a result, an amplification of the stimulated emission of the incident terahertz wave is obtained. Therefore, it can be said that the graphene plasmon instability can cause coherent resonant amplification of electromagnetic waves. We have successfully modeled the plasmonic electromagnetic response of the ADGG-GFETs and numerically verified the occurrence of THz self-excited oscillation phenomena originating from graphene plasmon instability (**Figure 5c**) [30].

3.2 Experiments

To demonstrate the light amplification of stimulated emission of THz radiation by excitation of graphene plasmons as described above, we fabricated a prototype ADGG-GFET with the help of 2-DTech Corp. Graphene sheets of the highest quality and hexagonal boron nitride (hBN), which is widely used as a chemically inert and mechanically stable material that less deteriorates graphene carrier transport, were deposited on bulk graphite and bulk hBN materials, respectively, by a peeling and transfer method and then sequentially. The hBN layer completely seals the top and bottom surfaces of the graphene channel. Source and drain electrodes were formed by edge-junction with graphene channels, whereas the gate electrodes were formed by electron beam lithography and a lift-off method. The amount of doping of the entire graphene channel can be back-gate controlled from the backside of the substrate. The finger length of the gate, which determines the plasmon resonance frequency, was differentiated between the two gates of the ADGG, and by selecting the gate that accumulates electrons when a high bias is applied, two resonator lengths can be evaluated in a single FET. Two prototype FETs with two different characteristic dimensions were evaluated for a total of four resonator structures C1 to C4 with different dimensions of 0.5, 0.75, 1.0, and 1.5 μm (**Figure 6a**). Measurements of the DC transfer characteristics confirmed the good ambipolar properties characteristic of bandgap-less graphene. The field-effect mobility extracted from the DC properties showed excellent values above 30,000 cm^2/Vs [13, 14].

The temporal response of the transmitted wave of the prototype ADGG-GFET to an incident terahertz pulse was measured by varying the DC voltage applied to the drain terminal using terahertz time-domain spectroscopy (TDS). To excite graphene plasmon resonance, in which the resonator structure is defined along with the shorter dimension corresponding to the gate finger of ADGG, it is necessary to align the polarization axis of the incident THz pulse in the channel direction. We controlled the incident terahertz pulse to be linearly polarized and verified the effect of plasmon excitation for two conditions: parallel and orthogonal polarization axes in the channel direction. All experiments were performed at room temperature.

First, the THz pulse response of ADGG-GFETs was measured with no drain bias applied. As a result, a strong resonant absorption property with an absorption rate exceeding a maximum of 16%, originating from a clear plasmon resonance, was measured only when the polarization axis of the incident terahertz pulse was aligned in the channel direction. When the polarization axis was orthogonal to the channel direction, a Drude absorption spectrum associated with free carrier absorption with a monotonically decreasing absorption rate with increasing frequency was observed (**Figure 6b**).

Next, the same experiment was conducted by gradually increasing the drain bias. As the drain bias increased, the resonance absorption decreased with a redshift (decrease in peak frequency). When the drain bias reached the first threshold level, the absorption turned to be fully transparent over the entire observed frequency band. When the drain bias was further increased to reach the second threshold, it turned into a resonant amplification characteristic. As the drain bias was further increased, the resonant amplification showed a blueshift (increase in peak frequency), and the amplification ratio increased up to 9% (**Figure 6c**). Asynchronous components such as self-excited oscillations associated with plasmon instability, for example, are not detected in principle. Therefore, the obtained amplification effect can be understood as a coherent light amplification of stimulated emission of the incident THz wave
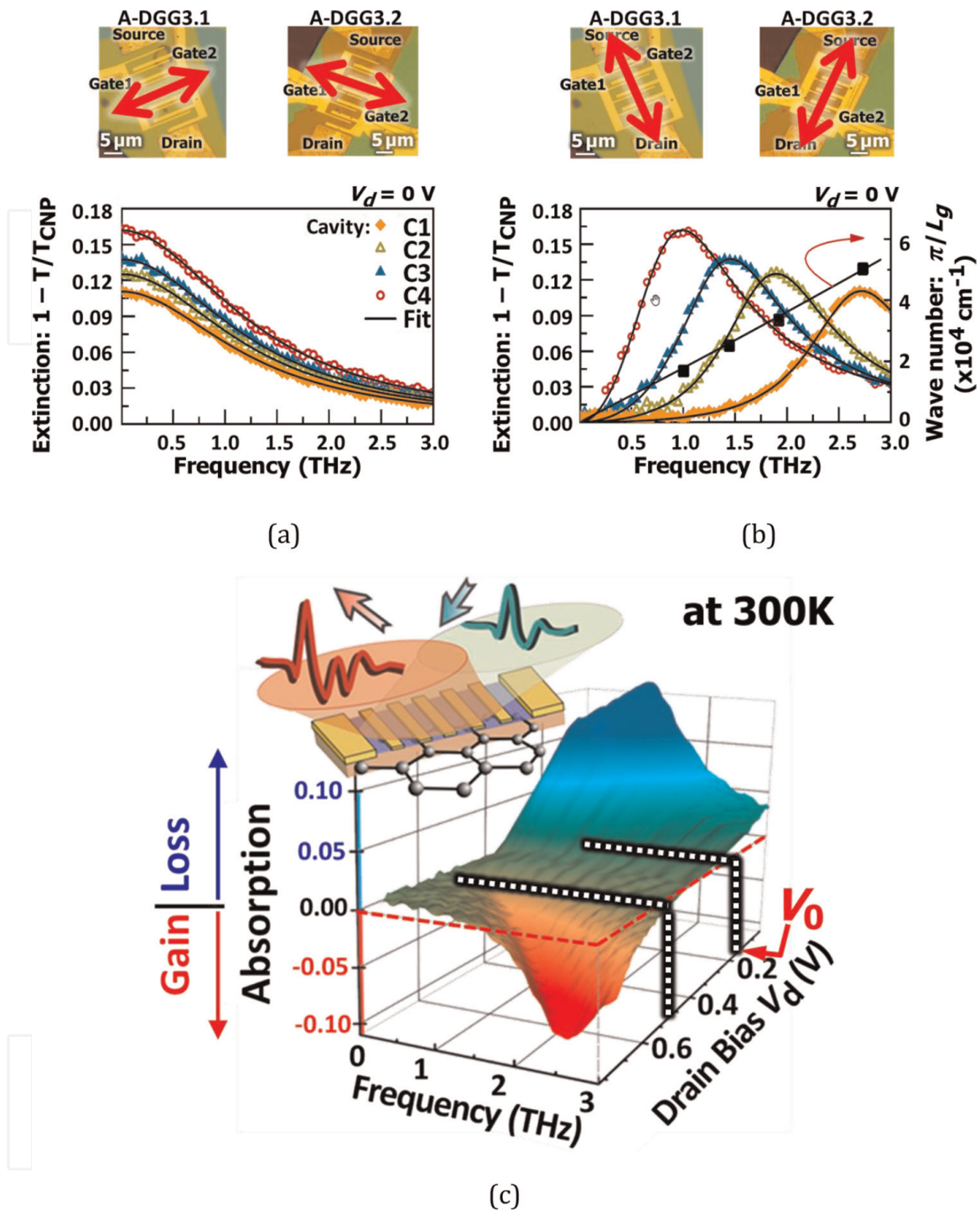
(a)

(b)

(c)

Figure 6.
Experimental results of THz temporal and frequency response of fabricated ADGG-GFETs using a TDS method. (a) Electron microphotographs of fabricated samples and their Drude-like absorption spectral characteristics under drain-unbiased conditions where plasmon is not excited with incident polarization (designated with red arrows) perpendicular to the ADGG finger. Adapted with permission by the authors under the Creative Commons Attribution CC-BY 4.0 International license from Ref. [13]. (b) Electron microphotographs of fabricated samples and their resonant absorption spectral characteristics under drain-unbiased condition where plasmon is excited with incident polarization (designated with red arrows) parallel to the ADGG finger. Adapted with permission by the authors under the Creative Commons Attribution CC-BY 4.0 IInternational license from Ref. [13]. (c) Resonant absorption and amplification spectral responses when drain biased is varied from 0 up to ~1 V.

radiation, in which the DC power energy supplied by the application of a DC drain bias is converted into an induced amplification component via the onset of plasmon instability.

The redshift observed in resonant absorption can be understood as the normal Doppler effect since the electron drift velocity increases with drain bias, while the blueshift observed in resonant amplification can be understood as the reverse Doppler effect. This effect means that the frequency response can be actively modulated and controlled by graphene, which is a discovery of a potential mean of new terahertz-band signal processing functionalities with a significant impact on the related engineering and industrial fields.

The experimental results of up to 16% absorption and 9% amplification of graphene greatly exceed the upper limit of quantum efficiency obtained by the direct interaction of photons of incident electromagnetic waves with graphene electrons, i.e., 2.3%, which corresponds to the optical absorption associated with direct interband transitions. The drain bias dependence of the obtained resonant dispersion properties is in good agreement with the properties in the plasmonic boom and Cherenkov-type instability that have been theoretically clarified. On the other hand, the drift velocity of graphene electrons with drain bias and the plasmon velocity were extracted, and the drift velocity was always lower than the plasmon velocity, suggesting that the operating mechanism of the plasmon instability is the expression of the D-S type and R-S-S type instabilities and that the plasmonic boom and Cherenkov-type instability were ruled out. In response to this contradiction, we newly modeled the plasmon dynamics of ADGG-GFETs and analyzed their properties, and found that the resonance dispersion properties observed even under conditions where the drift velocity does not exceed the plasmon velocity could be caused by the R-S-S type instability [13]. It is also suggested another possibility of the occurrence of a different type of new instability mechanism called Coulomb-drag instability of GDFs [31–33] of GDFs which we have recently discovered.

3.3 A discovery of a new instability mechanism in GFETs

Recently, we have discovered a new instability operating mechanism based on the Coulomb drag interaction of graphene Dirac plasmons [31–34]. The upper limit of the kinetic velocity of graphene Dirac fermions (GDFs) is defined by the slope of the band linear dispersion, i.e., the Fermi velocity $v_F (\approx 10^8 \text{ cm/s}$ even at RT$)$, which enables extremely high and micron-order long-distance ballistic transport even at room temperature [35]. At the same time, GDFs have extremely high viscosity, higher than that of honey, and the electron-to-electron scattering due to Coulomb interaction is extremely strong [36]. Due to these unique properties of GDFs, which are separated from the massive electrons in existing semiconductors, in the GFET structure with a channel length of less than a micron order under consideration, if GDFs are injected from the source end, they are transported in a ballistic manner in the ungated intrinsic region and reach the gate region with extremely high kinetic energy with the velocity of v_F. As a result, the quasi-equilibrium electrons (QEs) that aggregate in the gate region undergo strong Coulomb interaction with the ballistic transport electrons (BEs). Together with the high viscosity property of the GDFs, they are transformed into quasi-equilibrium drag electrons (DQEs) that enter a so-called drug state (**Figure 7a** and **b**) [31]. If the drain bias is applied weakly to the extent that the potential slope between the gate and drain is inverted from the slope of the forward potential between the drain and source, the inverted potential slope will cause QEs to be injected back into the channel from the drain end as depicted in **Figure 7a**. This has

Figure 7.
Coulomb-drag instability of graphene Dirac plasmons. (a) Bird's eye view of the device structure and related band diagram under a sufficient gate bias and a pertinent drain bias condition to promote the instability. Adapted with permission by Wiley-VCH GmbH from Ref. [32]. (b) Cross-sectional device structure and carrier flow. BE: ballistic electron, QE: quasi-equilibrated electron, DQE: dragged quasi-equilibrated Electron. (c) Typical channel current versus drain bias voltage at a gate-bias-dependent Fermi level of 60 meV for different temperatures of 10, 16, and 25 meV. Adapted with permission by American Physical Society from Ref. [31]. (d) Typical impedance when the Coulomb-drag instability is promoted in a GFET. The vertical axis is normalized to the i-region resistance. The fundamental plasmon resonant mode is characterized by the gated channel length and the electron density in the gated area at 1.07 THz. Adapted with permission by Wiley-VCH GmbH from Ref. [32].

the effect of reducing the channel current as the drain potential rises, resulting in negative differential conductivity (**Figure 7c**) [31, 32].

The channel currents consist of ballistic transport electron flow BE, quasi-equilibrium electron flow QE, and quasi-equilibrium drag electron flow DQE by

GDFs. Under such a situation, the current continuity was modeled by Kirchhoff's law, and the DC current-voltage characteristics and AC impedance were analytically obtained [31–33]. As a result, we theoretically discovered that, first, assuming micron-order GFET structure dimensions, extremely strong negative differential conductivity characteristics can be obtained in a wide THz band even at room temperature (**Figure 7c**) [31], and that the GFET gate region functions as a graphene plasmonic coherent oscillator in the THz frequency range (**Figure 7d**) [32, 33].

Second, in dual-gate GFETs, if a p-i-n junction is formed in the channel by applying complementary gate bias, the slope of the p-i-n junction with the application of drain bias becomes linear and steep, resulting in the valence electron holes in the p region and conduction electrons in the n region forming a Zener Klein tunneling [37], resulting in strong Coulomb drag as ballistic transport electron holes, and that this graphene tunneling transistor (GTT) also exhibits strong GDP Coulomb drag instability comparable to or stronger than that of single-gate GFETs (**Figure 8**) [34]. Moreover, the discovered instability has no high-speed requirement for carrier velocity in the plasmon resonator region, and the instability index under real device conditions is several times higher than other instabilities currently known (the Doppler-shifted D-S type, the Cherenkov-boom type, and the electron velocity modulation R-S-S type), and the prospect of achieving THz radiation intensity of 100 μW or higher under room temperature has been analytically demonstrated [34].

The Coulomb drag effect has been originally considered in a double-layered graphene structure in which two independent graphene are separated by an atomically thin insulation layer and electrostatically coupled working as a graphene nanocapacitor [38]. Our finding that the drag effect can take place even in a single graphene layer brings the effect into a simple GFET structure, diversifying its functionalities. In principle, the Coulomb drag mechanism can promote the plasma wave generation in the periodic GFET structures analogous to the previously considered two-stream instability systems with ballistic carrier flows and quasi-equilibrated non-traversing carriers in massive compound semiconductor heterostructures [39]. However, these classical massive 2D electron systems cannot totally mediate such a strong Coulomb drag effect as in GDFs due to their poor carrier transport properties. In summary, in the proposed GFET system, the critical differences and advantages over previous implementations are (i) the extraordinary transport properties of GDFs, which allow for ballistic transport over micrometers in graphene channels even at room temperature, and (ii) the strong Coulomb drag effect via the strong Coulomb inter-carrier scattering of GDFs.

3.4 Actively controlling the PT-symmetry of graphene Dirac plasmons

In quantum mechanics, it was discovered that even non-Hermitian Hamiltonians can provide realistic solutions if the system preserves the parity and time-reversal (PT) symmetries [40]. The author introduces active controlling of the PT symmetry to our original DGG-GFET structure by applied voltages and demonstrates a 100-Gbit/s-class ultrafast gain switching operation [11].

The PT symmetry can be expressed by a pair of complementary gain and loss mediums (**Figure 9**), leading to a perfect transmission property (unidirectionality) [41]. We first numerically confirmed such an anisotropic wave propagation in a PT-symmetric plasmonic metasurface by using a simple toy model of a transmission line consisting of a series of the unit kinetic-inductance/electrostatic-capacitance/Drude-conductance circuitry (**Figure 10a**), clearly reproducing the unidirectionality
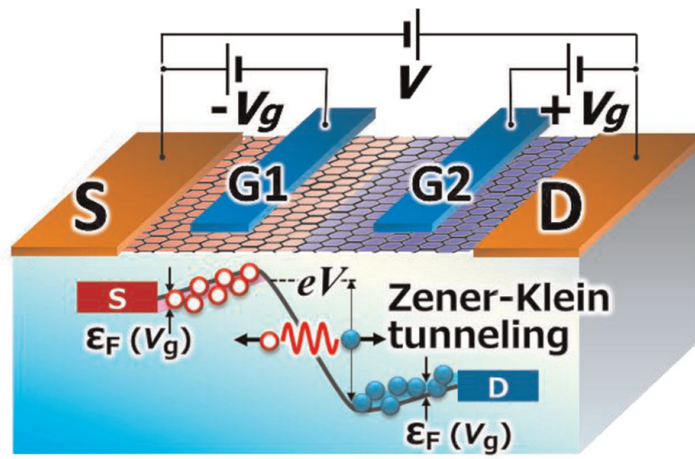
(a)
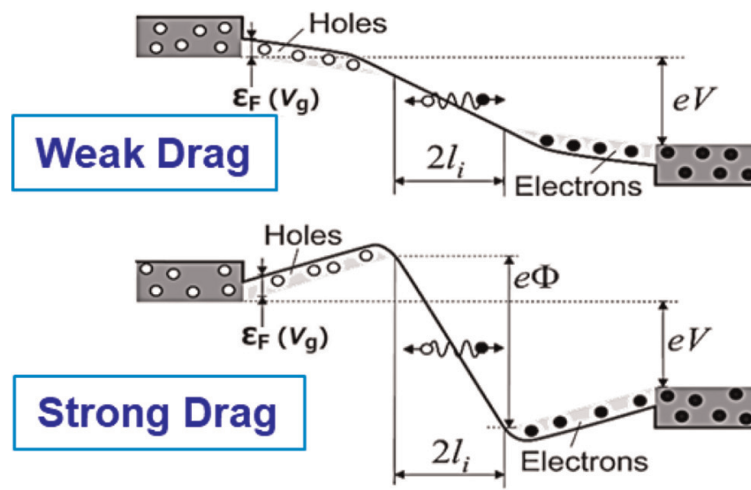
(b)
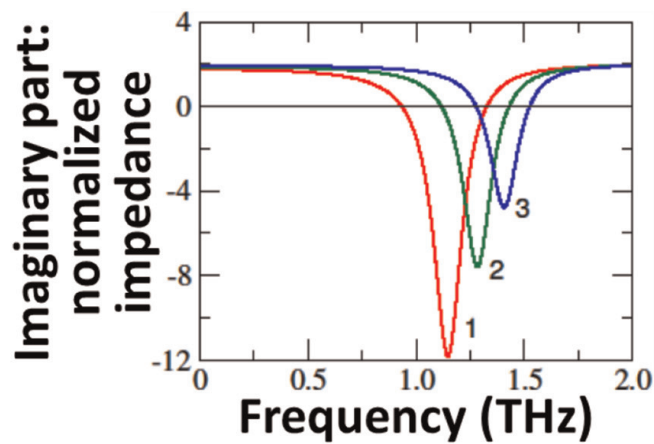
(c)

Figure 8.
Promotion of Coulomb-drag instability in a tunnel GFET. (a) Bird's eye view of the tunnel GFET structure and its band diagram under a strong drugged condition. (b) The change of the band diagram from a weak to a strong drag state. (c) Numerically calculated real part of the impedance normalized to the i-region resistance. Plots no. 1, 2, and 3 are the cases for the gate-bias-dependent plasmon mode frequency of 1.15, 1.3, and 1.4 THz, respectively. Adapted with permission by American Physical Society from Ref. [34].
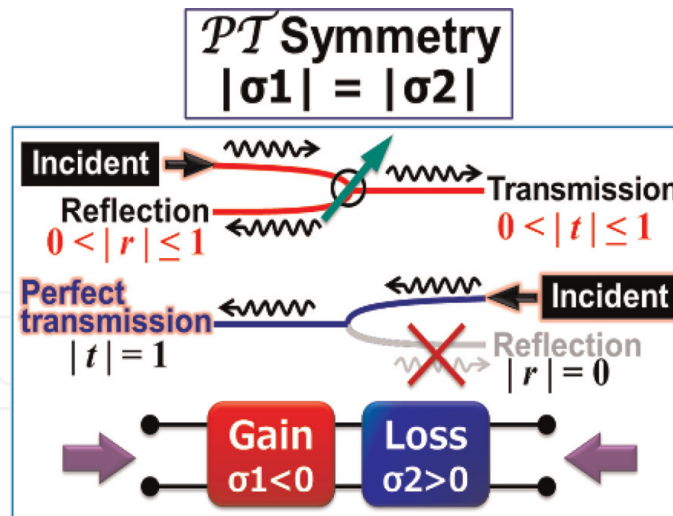
Figure 9.
Expression of the PT symmetric system in an electrically equivalent two-port circuit with a series of complementary gain and loss elements, demonstrating its unidirectionality of electromagnetic wave propagation having a normal transmission/reflection transmission when the signal is incident from the gain port and a perfect transmission when the signal is incident from the loss port. Adapted with permission by the authors under the Creative Commons Attribution CC-BY 4.0 International license from Ref. [11].

(a)   (b)
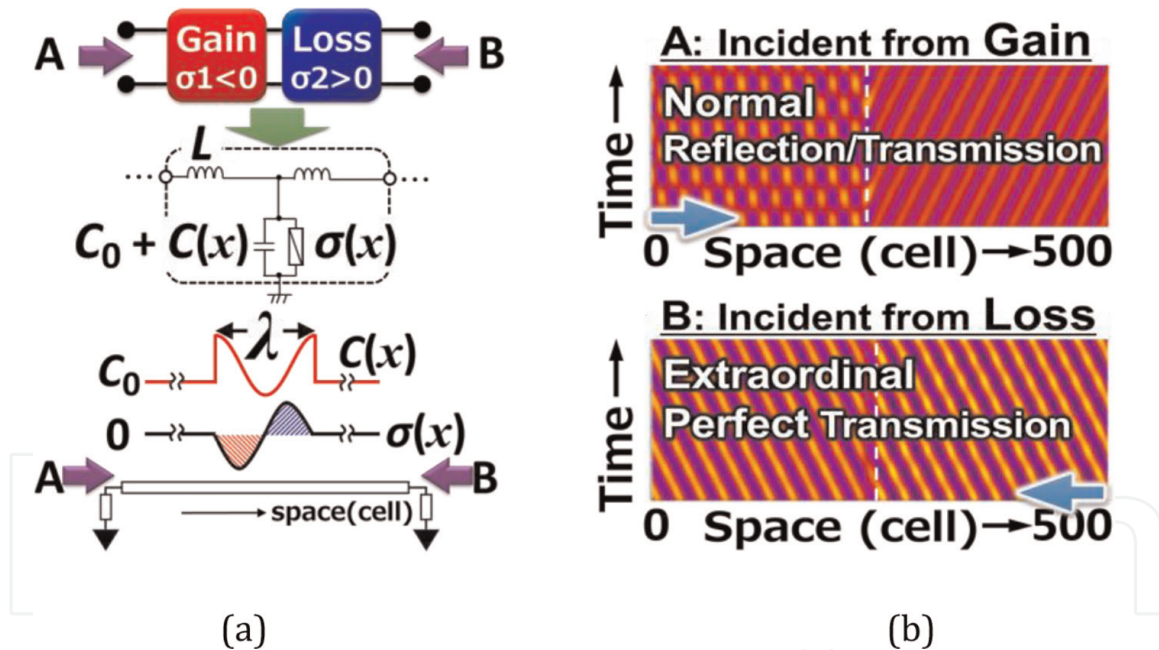
Figure 10.
Transmission line modeling of a PT-symmetric system and numerical analysis for reproducing is a unidirectionality characteristic. Adapted with permission by the authors under the Creative Commons Attribution CC-BY 4.0 International license from Ref. [11]. (A) A toy model for a PT-symmetric system in a distributed transmission line circuitry whose central core unit is given by the non-zero sinusoidal complementary gain-loss conductance element. (B) Spatio-temporal phase mapping of propagating the electromagnetic wave, demonstrating anisotropic, extraordinary perfect transmission when radiation is incident from the loss port.

(**Figure 10b**). When the GDPs in a DGG-GFET become unstable under forward-drain-biased, complementary DGG-biased conditions, the GDP metasurface is represented by a series connection of unit cells of the instability-driven gain section and the carrier-depleted loss section (**Figure 11**).
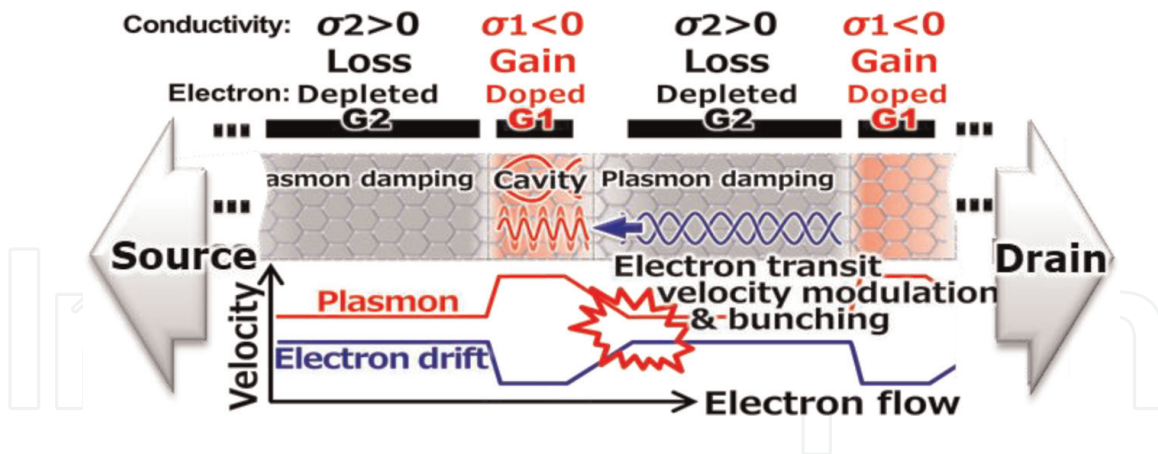
Figure 11.
Implementation of active control of the PT symmetry in a DGG-GFET in a case of R-S-S type GDP instability to be promoted. Adapted with permission by the authors under the Creative Commons Attribution CC-BY 4.0 International license from Ref. [11].

We numerically analyzed the transient response of a DGG-GFET to reveal how fast its laser cavity Q values are electrically controllable by using self-consistent simulation based on quasi-classical Boltzmann equation (**Figure 12**) [30]. The drain bias V_d was turned on at time zero. The electric field intensity, which is mainly applied to the depleted electron-transit region, was set at 0.8 kV/cm. The equivalent electron velocity
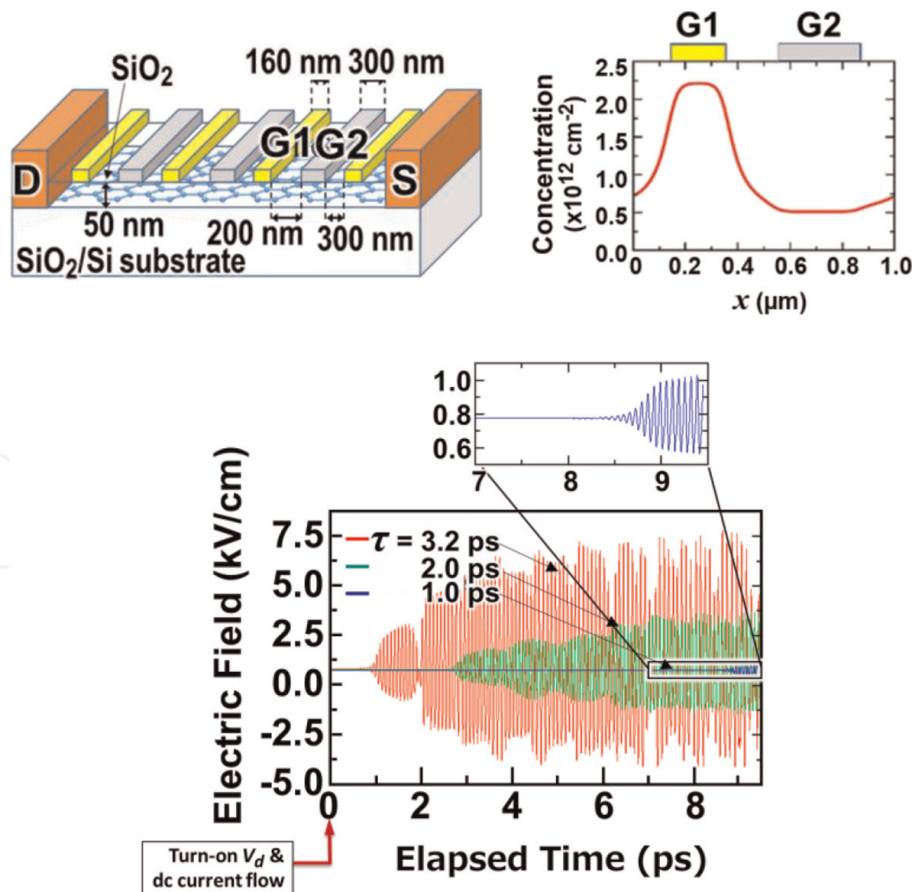
Figure 12.
Numerically simulated temporal evolution of GDP field activated by the dc-current-driven PT symmetry turned on at t = 0 ps for different momentum relaxation times τ of GDFs reaching the self-oscillation at the GDP mode frequency in a picosecond time scale. Adapted with permission by the authors under the Creative Commons Attribution CC-BY 4.0 International license from Ref. [11].
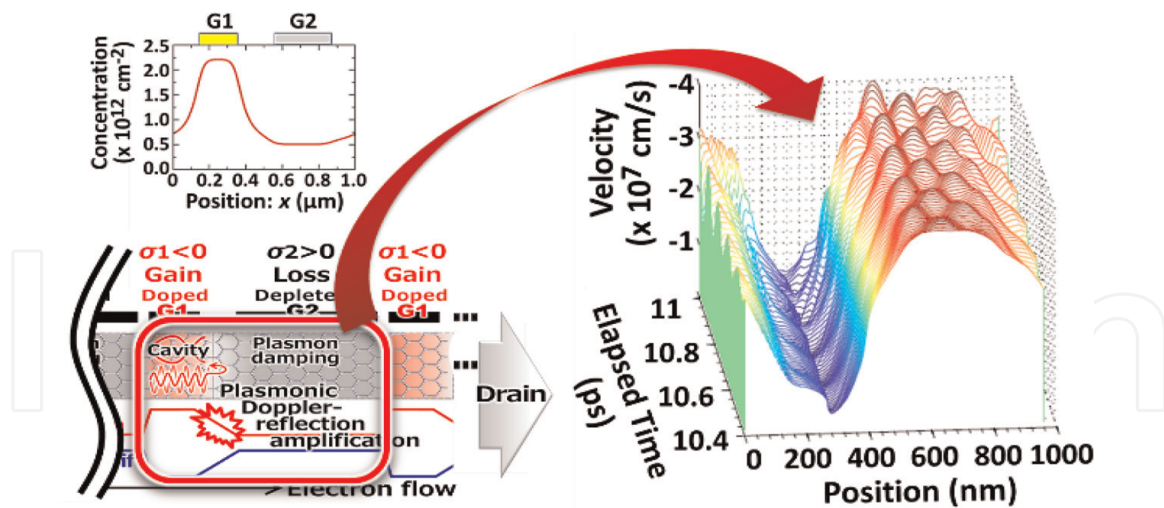
Figure 13.
Numerically simulated, temporally evolved spatial distribution of the carrier velocity in the DGG metasurface under THz self-oscillation promoted by the current-driven GDP instability. Adapted with permission by the authors under the Creative Commons Attribution CC-BY 4.0 International license from Ref. [11].

is estimated to be 4×10^7 cm/s at the field-effect mobility of 50,000 cm^2/Vs. **Figure 12** plots the temporal evolutions of the longitudinal electric field in the GDP cavity for τ = 1.0, 2.0, and 3.2 ps. Originally the graphene metasurface with zero-V_d is entirely lossy. With increasing V_d and the level of current injection pumping the GDP instability started to be promoted as is demonstrated in **Figure 6c**. When the instability-driven gain becomes balanced to the loss in the depleted region, the system becomes PT-symmetric. Further increase of V_d makes the level of instability-driven gain surpass that of the loss, resulting in THz self-oscillation of radiation emission. The important feature is its ultrafast transition speed within 10 ps duration. As is seen in **Figure 12**, the superior property with a longer τ value exhibits faster turning on with stronger field intensity of THz self-oscillation. Even for a rather moderate τ value of 1 ps the result demonstrates still fast transition to the stationary stage oscillation within 10 ps corresponding to the single-bit time slot for the 100 Gbit/s data rate.

    Figure 13 plots the temporal variations of the microscopic spatial distribution of the electron velocities in the unit cell of the GDP metasurface after more than 10 ps passed from the triggering where the field becomes the stationary state. The red-colored plotted region corresponding to the depleted region underneath G2 where GDFs travel fast clearly reproduces coherent oscillatory modulation, manifesting ignization of GDP-instability driven THz self-oscillation.

4. Possible scenario toward graphene plasmonic THz laser transistors operating at room temperature

    Based on the previous discussion, the author proposes a possible design of a graphene plasmon THz laser transistor based on the DGG-GFET structure as depicted in **Figure 14**. Suppose DGG G1 and G2 are complementary biased for bipolar (electron and hole) injection and forward biased between drain and source. The proposed device consists of a series of unit sections including the photonic seed section and the plasmon gain section. The photonic seed section generates spontaneous THz photons by current injection pumping, and the plasmon gain section amplifies the spontaneous
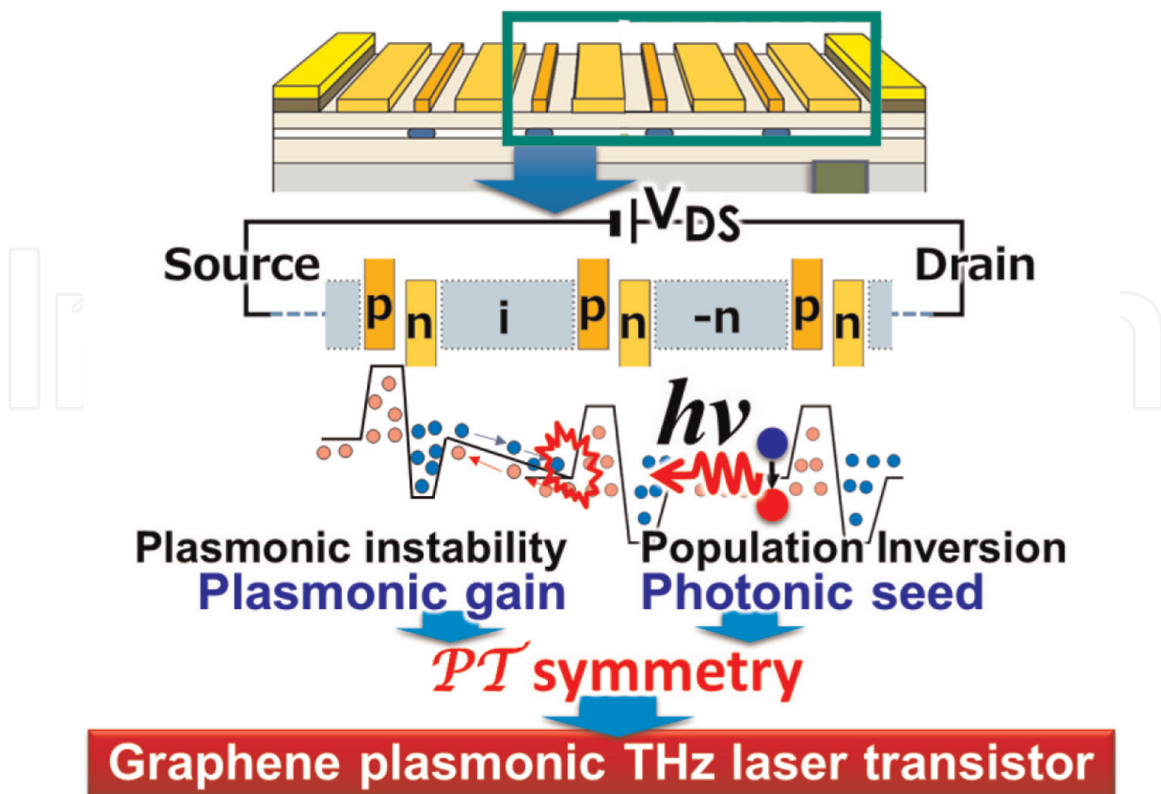
Figure 14.
A graphene plasmonic THz laser transistor structure of the author's proposal consisting of a series of unit sections including the photonic seed and the plasmonic gain sections. Adapted with permission by the authors under the Creative Commons Attribution CC-BY 4.0 International license from Ref. [11].

THz photons mediated by GDP instability. As described in Section 3.4, the idea of controlling the PT symmetry of the DGG-GFET metasurface helps to improve their performance and functionality such as ultrafast gain switching modulation.

The photonic seed section is selectively weakly doped (indicated by "-n" in **Figure 14**) in the wide ungated spacing of the photonic seed section to maintain a nearly flat band and retain inverted carriers in it under a slightly stronger drain bias voltage that promotes GDP instability in the plasmon gain section. This can be configured by selective weak n-type doping, but it may also be technically challenging. Electrostatic doping with back-gate biasing is a mature solution, but it is not easy with epitaxial graphene thermally decomposed on SiC substrates because it requires ultra-thin semi-insulating SiC substrates. Another method is chemical doping, but it has problems such as unintentional doping to other parts of the substrate, degrading the crystallinity, and shortening of carrier momentum relaxation time. Recently, a new technique has been developed to synthesize high-quality few-layer epitaxial graphene on single-crystalline SiC thin films grown on Si wafers [42]. Precise control of the epitaxially grown graphene layers also remains a challenge, which could be addressed by introducing microfabricated SiC substrate technology that can spatially limit the epitaxial area [43]. New ideas for such advanced devices and process technologies are the subject of future research.

5. Conclusions

In this chapter, the theory and experiments toward graphene-based plasmonic THz laser transistors were reviewed. The THz region is still under exploration due to

substantial physical limitations for both electron devices such as transistors and photonic devices such as lasers. Low-power consumed, integrated, room-temperature operating novel solid-state THz laser devices are the critical demand for a brighter future society. This is the reason why graphene, a monoatomic layer of sp2-bonded carbons in a honeycomb crystal lattice, has drawn attention due to its unique and superior carrier transport, optical, and plasmonic properties since it has been discovered in the mid-2000s. Electrons and holes in graphene hold a linear dispersive energy spectrum with zero bandgap, resulting in extraordinary features like massless relativistic Dirac fermions with back-scattering-free ultrafast transport as well as the negative-dynamic conductivity in the THz spectral range under optical or electrical pumping. The author's group succeeded in single mode emission at 5.2 THz and 1–8-THz broadband amplified spontaneous emission at 100 K from current-driven graphene-channel laser transistors. However, its gain and output intensity are thoroughly limited by the absorption coefficient of monolayer graphene below 2.3%. To break through the substantial limit, graphene Dirac plasmons (GDPs)opened a pathway toward the realization of intense THz laser transistors operating at room temperatures. The physics behind the GDPs is the current-driven instabilities giving rise to self-oscillation and coherent amplification in the THz electromagnetic spectra. The author's group designed and fabricated ADGG-GFETs and demonstrated room-temperature THz amplification with a maximum gain of 9% which was four times larger than the quantum mechanical limit when THz photons directly interact with GDFs via interband transition. The results obtained well suggested that these impactful results were due to the light amplification of stimulated emission of THz radiation promoted by the GDP instabilities. Active controlling the PT symmetry of the GDPs is a new impactful technological trend to be able to implement the ultrafast direct gain switching functionality to the graphene plasmonic THz laser transistors. Furthermore, the author's group discovered a new mechanism of instability in GDPs called Coulomb-drag instability. The theoretical analyses suggest that the amplification gain could exceed the level of other existing mechanisms of instability. At this moment, however, the new mechanisms of the last two topics have yet to be experimentally verified, which is expected to be disclosed in the near future.

Acknowledgements

Conflict of interest

The authors declare no conflict of interest.

Author details

Taiichi Otsuji
Tohoku University, Sendai, Japan

*Address all correspondence to: taiichi.otsuji.e8@tohoku.ac.jp

IntechOpen

References

[1] Sengupta K, Nagatsuma T, Mittleman DM. Terahertz integrated electronic and hybrid electronic–photonic systems. Nature Electronics. 2018;**1**: 622-635. DOI: 10.1038/s41928-018-0173-2

[2] Tonouchi M. Cutting-edge terahertz technology. Nature Photonics. 2007;**1**: 97-105. DOI: 10.1038/s41928-018-0173-2

[3] Tredicucci A, Vitiello MS. Device concepts for graphene-based terahertz photnics. IEEE Journal of Selected Topics of Quantum Electronics. 2014;**20**: 8500109. DOI: 10.1109/JSTQE. 2013.2271692

[4] Novoselov KS, Geim AK, Morozov SV, Jiang D, Zhang Y, Dubonos SV, et al. Electric field effect in atomically thin carbon films. Science. 2004;**306**:666-669. DOI: 10.1126/ science.1102896

[5] Geim AK, Novoselov KS. The rise of graphene. Nature Materials. 2007;**26**: 183-191. DOI: 10.1038/nmat1849

[6] Ando T, Fowler AB, Stern F. Electronic properties of two-dimensional systems. Reviews of Modern Physics. 1982;**54**:437-672. DOI: 10.1103/ RevModPhys.54.437

[7] Ryzhii V, Satou A, Otsuji T. Plasma waves in two-dimensional electron-hole system in gated graphene heterostructures. Journal of Applied Physics. 2007;**101**:024509. DOI: 10.1063/ 1.2326904

[8] Grigorenko AN, Polini M, Novoselov KS. Graphene plasmonics. Nature Photonics. 2012;**6**:749-758. DOI: 10.1038/NPHOTON.2012.262

[9] Ryzhii V, Ryzhii M, Otsuji T. Negative dynamic conductivity of graphene with optical pumping. Journal of Applied Physics. 2007;**83**:083114. DOI: 10.1063/1.2717566

[10] Ryzhii M, Ryzhii V. Injection and population inversion in electrically induced p-n junction in graphene with split gates. Japanese Journal of Applied Physics. 2007;**46**:L151-L153. DOI: 10.1143/JJAP.46.L151

[11] Otsuji T, Boubanga-Tombet SA, Satou A, Ryzhii M, Ryzhii V. Terahertz-wave generation using graphene: Toward new types of terahertz lasers. IEEE Journal of Selected Topics in Quantum Electronics. 2013;**19**:8400209. DOI: 10.1109/JSTQE.2012.2208734

[12] Yadav D, Tamamushi G, Watanabe T, Mitsuhio J, Tobah Y, Sugawara K, et al. Terahertz light-emitting graphene-channel transistor toward single-mode lasing. Nanophotonics. 2018;**7**:741-752. DOI: 10.1515/nanoph-2017-0106

[13] Boubanga-Tombet S, Knap W, Yadav D, Satou A, But DB, Popov VV, et al. Room temperature amplification of terahertz radiation by grating-gate graphene structures. Physical Review X. 2020;**10**:031004. DOI: 10.1103/ PhysRevX.10.031004

[14] Boubanga-Tombet AS, Satou A, Yadav D, But DB, Knap W, Popov VV, et al. Paving the way for tunable graphene plasmonic THz amplifiers. Frontiers in Physics. 2021;**9**:726806. DOI: 10.3389/fphy.2021.726806

[15] Dyakonov M, Shur M. Shallow water analogy for a ballistic field effect transistor: New mechanism of plasma wave generation by dc current. Physical Review Letters. 1993;**71**:2465. DOI: 10.1103/PhysRevLett.71.2465

[16] Ryzhii V, Satou A, Shur MS. Transit time mechanism of plasma instability in high electron mobility transistors. Physica Status Solidi A: Applications and Materials Science. 2005;**202**:R113. DOI: 10.1002/pssa.200521018

[17] Aizin GR, Mikalopas J, Shur M. Current-driven plasmonic boom instability in three-dimensional gated periodic ballistic nanostructures. Physical Review B. 2016;**93**:195315. DOI: 10.1103/PhysRevB.93.195315

[18] Mikhailov SA. Plasma instability and amplification of electromagnetic waves in low-dimensional electron systems. Physical Review B. 1998;**58**:1517. DOI: 10.1103/PhysRevB.58.1517

[19] Sano E. Monte Carlo simulation of ultrafast electron relaxation in graphene. Applied Physics Express. 2011;**4**:085101. DOI: 10.1143/APEX.4.085101

[20] Foster MS, Aleiner IL. Slow imbalance relaxation and thermoelectric transport in graphene. Physical Review B. 2009;**79**:085415. DOI: 10.1103/PhysRevB.79.085415

[21] Winzer T, Malic E. Impact of Auger processes on carrier dynamics in graphene. Physical Review B. 2012;**85**: 2410404(R). DOI: 10.1103/PhysRevB.85.241404

[22] Kim R, Perebeinos V, Avouris P. Relaxation of optically excited carriers in graphene. Physical Review B. 2011;**84**: 075449. DOI: 10.1103/PhysRevB.84.075449

[23] Someya T, Fukidome H, Watanabe H, Yamamoto T, Okada M, Sozuki H, et al. Suppression of supercollision carrier cooling in high mobility graphene on SiC(000¯1). Physical Review B. 2017;**95**:165303. DOI: 10.1103/PhysRevB.95.165303

[24] Alymov G, Vyurkov V, Ryzhii V, Satou A, Svintsov D. Auger recombination in Dirac materials: A tangle of many-body effects. Physical Review B. 2018;**97**:205411. DOI: 10.1103/PhysRevB.97.205411

[25] Dubinov AA, Aleshkin VY, Morozov SV, Ryzhii V, Otsuji T. Terahertz plasmon-emitting graphene-channel transistor. Opto-Electronics Review. 2019;**27**:345-347. DOI: 10.1016/j.opelre.2019.11.003

[26] Dubinov AA, Alehkin YV, Mitin V, Otsuji T, Ryzhii V. Terahertz surface plasmons in optically pumped graphene structures. Journal of Physics: Condensed Matter. 2011;**23**:145302. DOI: 10.1088/0953-8984/23/14/145302

[27] Watanabe T, Fukushima T, Yabe Y, Boubanga Tombet SA, Satou A, Dubinov AA, et al. The gain enhancement effect of surface plasmon polaritons on terahertz stimulated emission in optically pumped monolayer graphene. New Journal of Physics. 2013;**15**:075003. DOI: 10.1088/1367-2630/15/7/075003

[28] Ryzhii V, Otsuji T, Shur MS. Graphene based plasma-wave devices for terahertz applications. Applied Physics Letters. 2020;**116**:140501. DOI: 10.1063/1.5140712

[29] Popov VV, Fateev DV, Otsuji T, Meziani YM, Coquillat D, Knap W. Plasmonic terahertz detection by a double-grating-gate field-effect transistor structure with an asymmetric unit cell. Applied Physics Letters. 2011; **99**:243504. DOI: 10.1063/1.3670321

[30] Koseki K, Ryzhii V, Otsuji T, Popov VV, Satou A. Giant plasmon instability in a dual-grating-gate graphene field-effect transistor. Physical Review B. 2016;**93**:245408. DOI: 10.1103/PhysRevB.93.245408

[31] Ryzhii V, Ryzhii M, Mitin V, Shur MS, Otsuji T. S-shaped current-voltage characteristics of n+−i-n-n+ graphene field-effect transistors due the coulomb drag of quasi-equilibrium electrons by ballistic electrons. Physical Review Applied. 2021;**16**:014001. DOI: DOI

[32] Ryzhii V, Ryzhii M, Satou A, Mitin V, Shur MS, Otsuji T. Ballistic injection terahertz plasma instability in graphene n + −i-n-n + field-effect transistors and lateral diodes. Physica Status Solidi A. 2022;**219**:2100694. DOI: 10.1002/pssa.202100694

[33] Ryzhii V, Ryzhii M, Mitin V, Shur MS, Otsuji T. Coulomb electron drag mechanism of terahertz plasma instability in n+−i-n-n+ graphene FETs with ballistic injection. Applied Physics Letters. 2021;**119**:093501. DOI: 10.1063/5.0061722

[34] Ryzhii V, Ryzhii M, Satou A, Otsuji T, Mitin V, Shur MS. Effect of coulomb carrier drag and terahertz plasma instability in p+−p-i-n-n+ graphene tunneling transistor structures. Physical Review Applied. 2021;**16**:064054. DOI: 10.1103/PhysRevApplied.16.064054

[35] Mayorov AS, Gorbachev RV, Morozov SV, Britnell L, Jalil R, Ponomarenko LA, et al. Micrometer-scale ballistic transport in encapsulated graphene at room temperature. Nano Letters. 2011;**11**:2396-2399. DOI: 10.1021/nl200758b

[36] Bandurin DA, Torre I, Krishna Kumar R, Ben Shalom M, Tomadin A, Principi A, et al. Negative local resistance caused by viscous electron backflow in graphene. Science. 2016;**351**:1055-1058. DOI: 10.1126/science.aad0201

[37] Jena D. Tunneling transistors based on graphene and 2-D crystals. Proceedings of the IEEE. 2013;**101**: 1585-1602. DOI: 10.1109/JPROC.2013.2253435

[38] Gorbachev RV, Geim AK, Katsunelson MI, Novoselov KS, Tudorovskiy T, Grigorieva IV, et al. Strong coulomb drag and broken symmetry in double-layer graphene. Nature Physics. 2012;**8**:896-901. DOI: 10.1038/nphys2441

[39] Gribnikov ZS, Vagidov NZ, Mitin VV. Tow-stream instability and oscillatory regimes induced in ballistic diodes and field-effect transistors. Journal of Applied Physics. 2000;**88**: 6736-6745. DOI: 10.1063/1.1322383

[40] Bender CM, Boettcher S. Real spectra in non-Hermitian Hamiltonians having PT symmetry. Physical Review Letters. 1998;**80**:5243-5246. DOI: 10.1103/PhysRevLett.80.5243

[41] Ramezani H, Kottos T. Unidirectional nonlinear PT-symmetric optical structures. Physical Review A. 2010;**82**:04383. DOI: 10.1103/PhysRevA.82.043803

[42] Endoh N, Akiyama S, Tashima K, Suwa K, Kamogawa T, Kohama R, et al. High-quality few-layer graphene on single-crystalline SiC thin film grown on affordable wafer for device applications. Nanomaterials. 2021;**11**:392. DOI: 10.3390/nano11020392

[43] Fukidome H, Kawai Y, Fromm F, Kotsugi M, Handa H, Ide T, et al. Suemitsu M: Precise control of epitaxy of graphene by microfabricating SiC substrate. Applied Physics Letters. 2012; **101**:041605. DOI: 10.1063/1.4740271